

## Aluto-Langano Geothermal Field, Ethiopia: Complete Image Of Underlying Magmatic-Hydrothermal System Revealed By Revised Interpretation Of Magnetotelluric Data

Friedemann Samrock<sup>1</sup>, Alexander V. Grayver<sup>2</sup>, Biruk Cherkose<sup>3</sup>, Alexey Kuvshinov<sup>2</sup>, Martin O. Saar<sup>1</sup>

Mailing address, 1. Geothermal Energy and Geofluids Group, Institute of Geophysics, Sonneggstrasse 5, CH-8092 Zurich, Switzerland. 2. Earth and Planetary Magnetism, Institute of Geophysics, Sonneggstrasse 5, CH-8092 Zurich, Switzerland, 3. Geological Survey of Ethiopia, Addis Ababa Ethiopia

E-mail address, fsamrock@ethz.ch

**Keywords:** Geothermal exploration, Magnetotellurics, High-enthalpy geothermal systems, Volcano monitoring, Ethiopia

### ABSTRACT

Aluto-Langano in the Main Ethiopian Rift Valley is currently the only producing geothermal field in Ethiopia and probably the best studied prospect in the Ethiopian Rift. Geoscientific exploration began in 1973 and led to the siting of an exploration well LA3 on top of the volcanic complex. The well was drilled in 1983 to a depth of 2144m and encountered temperatures of 320°C. Since 1990 Aluto has produced electricity, albeit with interruptions. Currently it is undergoing a major expansion phase with the plan to generate about 70MWe from eight new wells, until now two of them have been drilled successfully.

Geophysical exploration at Aluto involved magnetotelluric (MT) soundings, which helped delineate the clay cap atop of the hydrothermal reservoir. However, until now geophysical studies did not succeed in imaging the proposed magmatic heat source that would drive the observed hydrothermal convection.

For this study, we inverted 165 of a total of 208 MT stations that were measured over the entire volcanic complex in three independent surveys by the Geological Survey of Ethiopia and ETH Zurich, Switzerland. For the inversion, we used a novel 3-D inverse solver that employs adaptive finite element techniques, which allowed us to accurately model topography and account for varying lateral and vertical resolution. We inverted MT phase tensors. This transfer function is free of galvanic distortions that have long been recognized as an obstacle in MT inversion.

Our recovered model shows, for the first time, the entire magmatic-hydrothermal system under the geothermal field. The up-flow of melt is structurally controlled by extensional rift faults and sourced by a lower crustal basaltic mush reservoir. Productive wells were all drilled into a weak fault zone below the clay cap. The productive reservoir is underlain by an electrically conductive upper-crustal feature, which we interpret as a highly crystalline rhyolitic mush zone, acting as the main heat source. Our results demonstrate the importance of a dense MT site distribution and state-of-the-art inversion tools in order to obtain reliable and complete subsurface models of high enthalpy systems below volcanic geothermal prospects.

### 1. INTRODUCTION

The Ethiopian Rift Valley is one of the privileged areas for potential geothermal energy extraction, including electric power generation. As of yet, 22 areas have been discovered within the scope of a geothermal development program in Ethiopia that began four decades ago (Kebede, 2016; Hochstein et al., 2017). The prospects host geothermal resources suitable for electricity generation with a total estimated potential of more than 10'000MWe (Kebede, 2016).

In the central Main Ethiopian Rift (MER) the most promising geothermal sites are all located along a narrow network of *en echelon* disposed NNE-SSW trending faults, known as the Wonji fault belt (WFB) (e.g. Corti, 2009; Ebinger et al., 2017). The WFB is the main center of present-day rifting with spreading velocities that reach up to 5mm/year (Birhanu et al., 2016). Here, accumulated, rifting-related stresses are episodically released or redistributed by means of faulting and magmatic intrusion, resulting in distinct zones of magmatism. Volcanism along the WFB formed large peralkaline silicic volcanic complexes that include Corbetti, Aluto and Tulu Moye in the southern Lake District. The three volcanic sites are associated with a high geothermal activity that manifests itself in surface features comprising boiling hot springs, steam vents and areas with fumarolic activity that hint on ongoing active magmatic processes in the subsurface.

However, despite the long history of geothermal programs in the country, Aluto-Langano at Aluto volcano is the only geothermal field, which has been developed until now. A pilot power plant was installed in 1998 with a net capacity of 7.3MWe using two productive wells. Since then it has produced (albeit intermittently) electric power (Hochstein et al., 2017). Currently, expansion work is ongoing to increase the installed capacity to 70MWe and two new production wells have already been successfully drilled (Sisay, 2016). In 2018, geothermal energy utilization in Ethiopia experienced a boost in development and contracts were signed to install geothermal power generation facilities with a total capacity of more than 1000MWe at the two hitherto untapped geothermal fields of Corbetti and Tulu Moye (Press Release Reykjavik Geothermal Ltd.).

Geothermal exploration at Aluto began in the late 70s and led to the siting of the first productive exploration well, LA3, on top of the volcanic complex (see Fig. 1). The well was successfully drilled in 1983 (Hochstein et al., 2017). Early exploration studies involved DC-resistivity soundings with large electrode spacings of up to 3.15km and sections measured across and around the volcanic complex. Soundings on top of the Aluto dome commonly revealed an electrically resistive top layer (>30Ωm), with a thickness of up to 300m. Below the top layer measurements encountered a layer with low electrical resistivities (<6Ωm). As confirmed later by drilling, the resistive top layer consists of dry unconsolidated pyroclastics, silicic tuff and breccia (Hochstein et al., 2017). The

electrically conductive layer represents the clay cap, which is typically found in high-enthalpy geothermal systems (Johnston et al., 1992). Here, high electrical conductivities are caused by smectite clays, that are produced by argillic alteration taking place in hydrothermal reservoirs at temperatures roughly below 250°C (Levy et al., 2018). The first productive well, LA3, was drilled on top of the volcanic complex into a fault zone that dissects the volcanic complex in an NNE-SSW direction parallel to the WFB. This zone, also known as the Artu Jawe Fault Zone (AJFZ), was identified as the main structural control that facilitated past volcanic eruptions (Hutchison, 2015). Aligned vents and CO<sub>2</sub>-degassing reach a maximum over the AJFZ and are indicative of this structure controlling present day upflow of geothermal fluids (Hutchison et al., 2015). Well LA3 encountered maximum temperatures of 336°C with boiling conditions from a depth of 700m below the smectite clay cap down to the bottom hole at 2144m (Gianelli and Teklemariam, 1993). In 2015, two new productive wells, LA9 and LA10, were drilled into the AJFZ during an expansion project, which aims at increasing the net capacity of the power plant to 70 MWe (Sisay, 2016).

The first wells, LA1 and LA2, were drilled south and west of the volcanic complex (Fig. 1b). Both ended up being non-productive and were affected by temperature reversals and cooling due to lateral inflow of cold water. The LA1 and LA2 wells are considered to be drilled into the outflow zone of the geothermal system. Resistivity soundings around LA1 and LA2 found a thin (<50m) resistive top layer (>100Ωm) that is underlain by a low electrical resistivity layer (<10Ωm) down to the lower sounding depths of a few hundred meters (Hochstein et al., 2017). Well logs show that the low resistivities are explained by the presence of lacustrine sediments and low-temperature thermal alteration in the basaltic layers at depths below 700m (Hochstein et al., 2017).

Thanks to a study by Biggs et al. (2011), who discovered that active ground deformations take place at Aluto, the geothermal prospect attracted interest and several geophysical surveys were performed to identify the source of the observed deformation. Using Interferometric Synthetic Aperture Radar (InSAR) satellite remote sensing techniques, Biggs et al. (2011) identified several cycles of uplift and setting that took place within the observation period from 2003 to 2010. For this study we derived surface deformation time series for an uplift event during the second half of the year 2008, using the grid processing on demand (G-POD) tool, provided by the European Space Agency (Casu et al., 2014). The deformation velocities for this event are shown in Fig. 1b. As can be seen, the maximum surface deformation occurs above the upflow zone of the geothermal system, where the productive wells are drilled. However, there is no evidence that the observed ground deformations are related to geothermal energy production at Aluto, but rather caused by a deeper source at about 5000m below the land surface (Hutchison et al., 2016).

Geophysical prospecting at Aluto involved magnetotelluric (MT) soundings that are capable of imaging the electrical resistivity of the Earth at a depth range from the shallow crust down to the upper mantle (e.g. Simpson and Bahr, 2005). At Aluto, MT studies were performed by the Geological Survey of Ethiopia (GSE) for geothermal exploration purposes in 2009 (Cherkose et al., 2018) and in 2012 by ETH Zurich in a study that aimed at identifying the source of unrest (Samrock et al., 2016). With their investigations, the surveys concentrated on the central part of the volcanic complex, where the productive wells were drilled (see Fig 1a). In 2015, a third MT campaign was conducted by the GSE, covering the entire volcanic complex (Rizello et al., 2017).

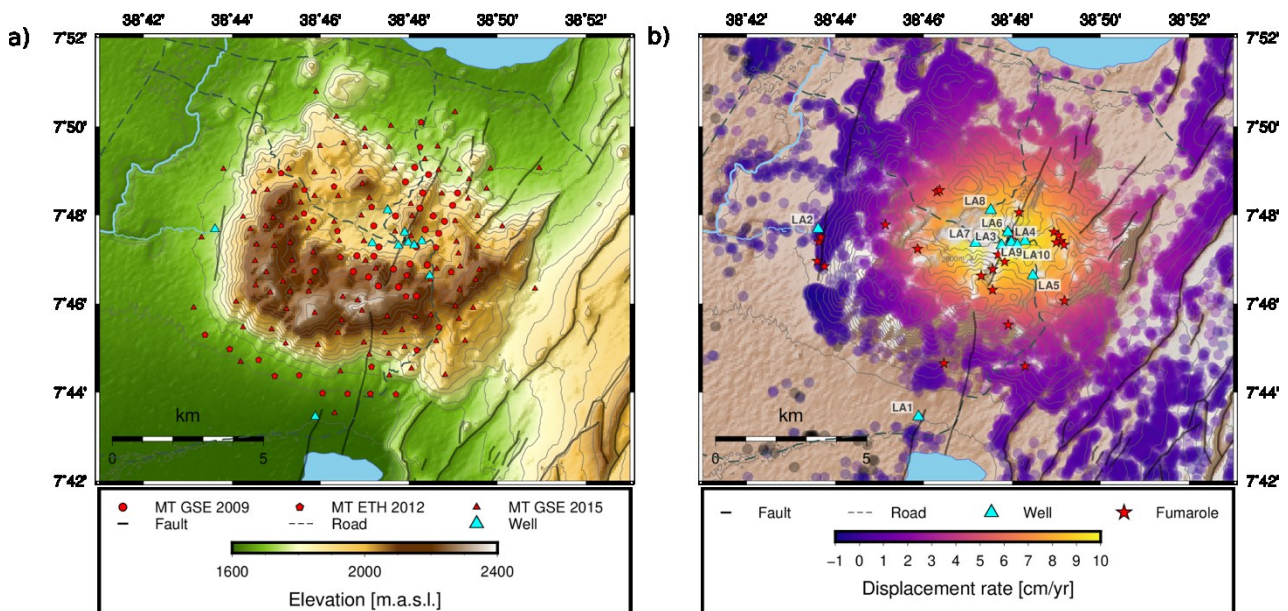


**Figure 1: Maps of the Aluto volcanic complex between the Lakes Ziway (North) and Langano (South). a) Distribution of measured MT site locations used for this study. b) Surface displacement rate in the satellite line of sight (LOS), obtained from Interferometric Synthetic Aperture Radar (InSAR) data for the uplift event from January to December 2008.**

3-D electrical resistivity models, recovered with the MT studies, showed in overall a good agreement with data from well logs. The models particularly helped to map the extent of the electrically conductive clay cap and the more resistive propylitic alteration zone into which the four productive wells (LA3, LA6, LA9 and LA10) have been drilled. However, no evidence was found for the existence of a crustal conductor as one would expect if an active magmatic system with significant amounts of melt was present under Aluto. Based on the analysis of tipper transfer functions that contain information about lateral electrical conductivity variations, Samrock et al. (2016) proposed that the dominating conductor in this region of the MER is located about 40km west of Aluto beneath an off-rift volcanic belt. This was later confirmed by Hübner et al. (2018), who conducted a cross-rift MT survey. However, like the studies

before, their study did not provide evidence for the existence of a strong electrical conductor and, thus, significant amounts of melt, beneath Aluto.

For this study we collected the data of all 208 MT stations that were measured at Aluto over the past years and inverted them using a novel 3-D inverse solver by Grayver (2015). Our data selection comprises a total of 165 MT stations that are distributed over the entire volcanic complex (Fig. 1a). Sites with poor data quality and identical locations were excluded.

## 2. METHOD

The standard transfer function in MT is the impedance tensor,  $\mathbf{Z}$ , which relates the horizontal electric and magnetic fields recorded at a specific location,  $\mathbf{r}$ , at the Earth's surface. In the frequency domain, it represents a complex-valued, second-rank tensor given by

$$\begin{pmatrix} E_x(\mathbf{r}, \omega) \\ E_y(\mathbf{r}, \omega) \end{pmatrix} = \begin{pmatrix} Z_{xx}(\mathbf{r}, \omega) & Z_{xy}(\mathbf{r}, \omega) \\ Z_{yx}(\mathbf{r}, \omega) & Z_{yy}(\mathbf{r}, \omega) \end{pmatrix} \begin{pmatrix} H_x(\mathbf{r}, \omega) \\ H_y(\mathbf{r}, \omega) \end{pmatrix} \quad (1)$$

where  $E_i$  and  $H_i$  ( $i \in [x, y]$ ) are the electric and magnetic field variations, respectively, measured in the North (x) and East (y) directions and  $\omega$  is the angular frequency.  $\mathbf{Z}$  is typically measured for a wide frequency range and contains information about the subsurface electrical conductivity structure at different depths. Penetration depth,  $d$ , of the electromagnetic variations depends on frequency,  $\omega$ , and the subsurface electrical conductivity,  $\sigma$ , thereby providing a means for sounding. The tensor elements,  $Z_{ij}$ , are usually displayed in terms of the apparent resistivity,  $\rho_a$ ,

$$\rho_{a_{ij}}(\mathbf{r}, \omega) = \frac{1}{\mu_0 \omega} |Z_{ij}(\mathbf{r}, \omega)|^2, \quad (2)$$

where  $\mu_0$  is the magnetic permeability of free space, and the phase  $\phi$  is given by

$$\phi_{ij}(\mathbf{r}, \omega) = \arctan\left(\frac{\text{Im}(Z_{ij}(\mathbf{r}, \omega))}{\text{Re}(Z_{ij}(\mathbf{r}, \omega))}\right). \quad (3)$$

The impedance tensor is often affected by galvanic distortions, which are caused by small-scale near surface heterogeneities near the measurement location,  $\mathbf{r}$ , leading to charge accumulation at conductivity interfaces and causing a bias in measured electric fields (Jiracek, 1990).

Galvanic distortions of the electric field can be described mathematically by a frequency-independent, real-valued, second rank distortion tensor,  $\mathbf{D}$ , which translates into a distorted impedance tensor,  $\mathbf{Z}_D$ :

$$\mathbf{E}_D(\mathbf{r}, \omega) = \mathbf{Z}_D(\mathbf{r}, \omega) \mathbf{H}(\mathbf{r}, \omega) = \mathbf{D}(\mathbf{r}) \mathbf{Z}(\mathbf{r}, \omega) \mathbf{H}(\mathbf{r}, \omega), \quad (4)$$

where  $\mathbf{Z}$  is the undistorted impedance tensor and the subscript D denotes distorted quantities. If not accounted for, galvanic distortions may result in subsurface artefacts during inversion (Tietze et al., 2015), possibly leading to erroneous interpretations.

Caldwell et al. (2004) introduced the MT phase tensor,  $\Phi$ , a transfer function, which can be deduced from the impedance tensor as follows (hereinafter, the frequency,  $\omega$ , and site location,  $\mathbf{r}$ , are omitted for brevity):

$$\Phi = \mathbf{X}^{-1} \mathbf{Y}, \quad (5)$$

where  $\mathbf{X}$  and  $\mathbf{Y}$  are the real and the imaginary parts of the impedance tensor  $\mathbf{Z} = \mathbf{X} + i\mathbf{Y}$ . It can be easily shown that  $\Phi$  is free from galvanic distortion,

$$\mathbf{X}_D^{-1} \mathbf{Y}_D = (\mathbf{D} \mathbf{X}^{-1}) (\mathbf{D} \mathbf{Y}) = \mathbf{X}^{-1} \mathbf{D}^{-1} \mathbf{D} \mathbf{Y} = \mathbf{X}^{-1} \mathbf{Y}, \quad (6)$$

where  $\mathbf{X}_D$  and  $\mathbf{Y}_D$  are the distorted real and imaginary parts of the impedance tensor. 3-D phase tensor inversion has not yet established itself in MT analyses, however, a few studies demonstrated its advantages in interpreting MT responses that are affected by galvanic distortions (Tietze et al., 2015; Samrock et al., 2018).

For the numerical inverse modeling of the data we used GOFEM – a 3-D inversion code that is based on the finite-element technique that exploits frequency-dependent automatic mesh refinement techniques for both forward and inverse modelling (Grayver, 2015; Grayver et al. 2019). As a result, GOFEM enables the modeling of realistically complex geological structure and the accurate incorporation of true topography, which is crucial to account for topography effects in the MT data (Käufel et al., 2018). Note, the terrain in our study area is characterized by a pronounced relief, with elevations that range from about 1600 to 2400 m.a.s.l.. Besides the standard MT responses (eqs. 1-3), GOFEM can invert in 3-D for phase tensors (eq. 5) to avoid problems that arise from galvanic distortions.

## 3. RESULTS AND INTERPRETATION

We obtained 3-D subsurface electrical resistivity models by inversion of full MT phase tensors at the selected 165 sites. The data cover a period range from 0.0173s to 1000s. Errors were propagated from the impedance tensor estimates, with an applied error-floor of  $0.05 \sqrt{|Z_{xy}|^2}$  for the elements  $Z_{xy}$  and  $Z_{xx}$  and  $0.05 \sqrt{|Z_{yx}|^2}$  for the elements  $Z_{yx}$  and  $Z_{yy}$ . Note, by row-wise application of the

error-floor, one avoids mis-scaled errors in case of either  $E_x$  or  $E_y$  being galvanically distorted. The complete inversion procedure is described in the Supporting Information in Samrock et al. (2018).

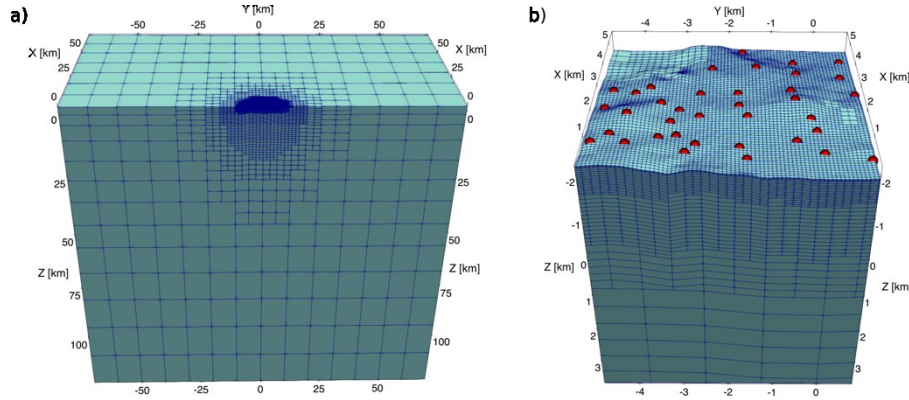


**Figure 2: Mesh used for the inversion. a) Overall modeling region. MT stations are located in the center of the mesh. The varying cell size accounts for the lower resolution of the MT method away from the stations. b) Detailed view of the central mesh region with topography-conforming mesh and observation sites (red dots). The depth level  $z=0$ km corresponds to the mean sea level.**

The mesh we used for the inversion accounts for the decreased resolution of MT data at depth with a coarser parameterization (Fig. 2a). We implemented true NASA SRTM topography data into the model with the highest resolution close to the MT site locations (Fig. 2b).

The best fitting model converged from an initial rms misfit of 2.97 to 0.93. Overall the inversion reached a good fit and residuals are uniformly distributed, hence, a geological interpretation of the model is justified. Fig. 3 shows an EW-slice of the recovered electrical conductivity model together with the borehole trajectories.

The upper crustal conductor, C1, corresponds to the clay cap, respectively the argillic alteration zone. This zone was already identified in previous MT surveys (Samrock et al., 2016; Cherkose et al., 2017, Cherkose et al., 2018). As confirmed by well stratigraphy analyses, low electrical resistivities in C1 are caused by smectite clays that form by hydrothermal alteration (Gianelli and Teklemariam, 1993). The electrical conductor, C2, west of Aluto is related to lake sediments, saline fluids and, in the deeper basaltic

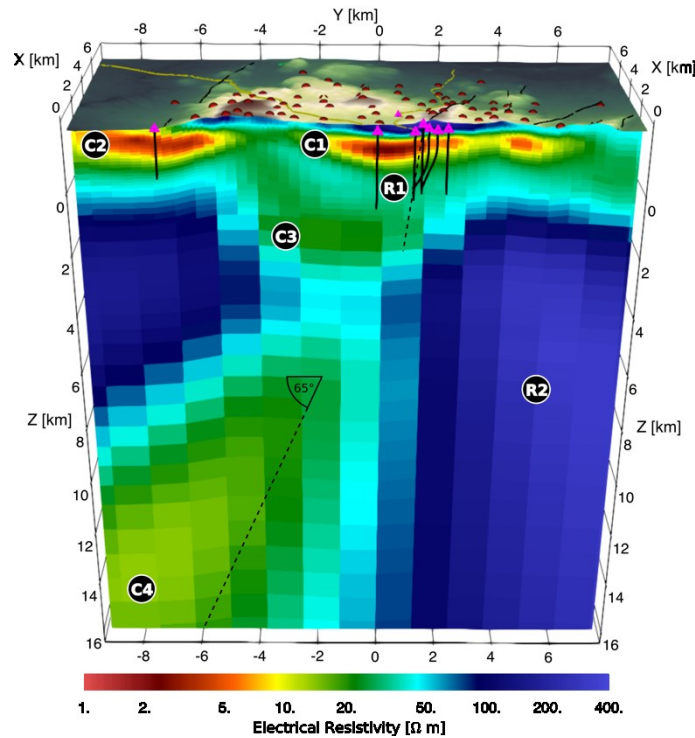


**Figure 3: EW-slice through the recovered electrical resistivity model. The surface layer shows SRTM topography data. Red dots mark MT site locations, black lines faults and yellow lines roads. Dashed lines indicate the orientation of fault planes in the subsurface. Wells and their trajectories are marked by magenta triangles and black lines, respectively. C1 to C4 and R1 to R2 mark prominent features as discussed in the main text.**

layer, thermally altered rocks, altered by old paleo-thermal out-flows (Hochstein et al., 2017). A relatively resistive zone, R1, is located under C1, that was identified as the propylitic alteration zone, where thermally altered products have higher electrical resistivities. This zone is tapped by the productive wells LA3, LA6, LA9 and LA10.

A new feature, that has not yet been imaged in previous MT studies, is the electrical conductor C3, which is located approximately between 1000 and 3000 m.b.s.l.. C3 is centered under a region, which was only sparsely covered in previous MT surveys by the GSE in 2009 and ETH in 2012 (Fig. 1a). At greater depths below 6000 m.b.s.l., another conductive feature C4 appears, that follows a proposed fault plane at an angle of the steep border faults found in this area of the MER. Also, this feature was not yet clearly imaged in previous local and regional MT studies (e.g. Samrock et al., 2016; Cherkose 2018; Hübert et al., 2018).

It is likely that C3 represents a former rhyolitic melt reservoir, as it was imaged below the Tulu Moye geothermal prospect (Samrock et al., 2018). Below Aluto, however, the upper crustal melt zone appears to be relatively resistive ( $\sim 15\text{-}25\Omega\text{m}$ ), which can be explained by only a low partial melt fraction as one expects for a highly crystalline former partial melt reservoir. Gleeson et al. (2017) modelled the melt evolution at Aluto using petrological constraints from local magmatic rock samples. In their study Gleeson et al. (2017) constrain pre-eruptive conditions of per-alkaline rhyolites at Aluto as summarized in Table 1.

Pressure	150MPa
Temperature range	718-765°C
H <sub>2</sub> O-content	5wt%

**Table 1: Pre-eruptive per-alkaline rhyolite melt conditions at Aluto as inferred by Gleeson et al. (2017).**

For this study we used the pressure conditions at depth of the imaged conductor, C3 (110MPa, 4km). Allowing a water content of 3-5wt% and using the rhyolite melt model by Guo et al. (2016), melt electrical resistivities at Aluto for the above-mentioned conditions range from  $0.75\Omega\text{m}$ , for melt with a high water-content and temperature, to  $1.2\Omega\text{m}$ , for low water contents and low temperatures (Fig 4a). Using this as constraint for melt resistivities, we estimated the melt content in C3 (with an electrical resistivity of  $20\text{-}25\Omega\text{m}$ ), using a two-phase Archie's law to relate bulk rock resistivities and melt resistivities whilst taking into account the interconnectivity of the melt (Glover et al., 2000). The interconnectivity is described by the cementation exponent,  $m$ , which, for connectivities at the upper Hashin-Shtrikman bound, is  $m=1.15$ . Crystalline mush is represented by a cementation exponent of about  $m=1.5$ . Using these constraints, we inferred the rhyolite melt fraction in the imaged upper crustal reservoir to range from very low melt fractions of 4.5% to higher melt fractions of up to 15%. The smaller melt fraction represents the case for maximum water content, temperature and melt connectivity. Higher melt fractions are required if one assumes a lower water content, temperature and poorly interconnected melt (see Fig 4b).

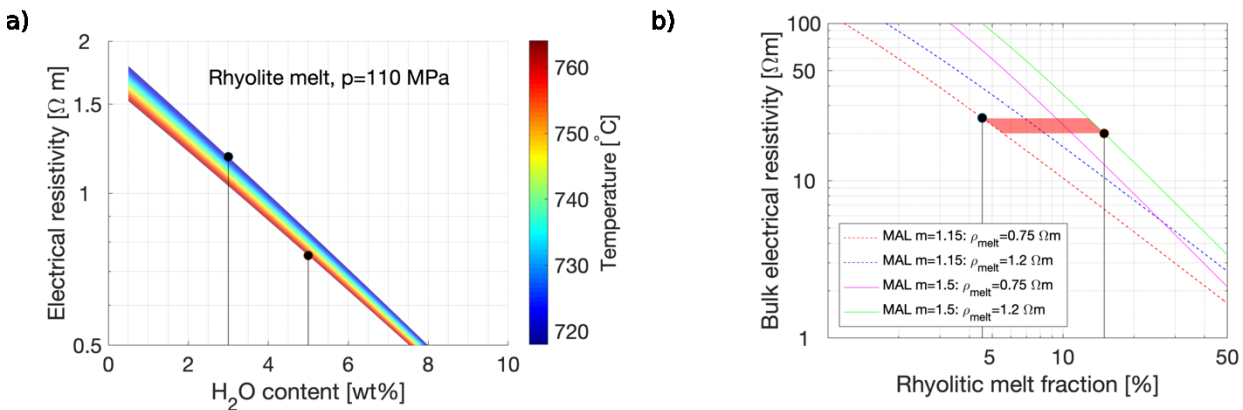


**Figure 4: a) Electrical resistivity of rhyolitic melt as a function of H<sub>2</sub>O-content and temperature at a given pressure of 110MPa, using the melt model by Guo et al. (2016). For this study, we use the boundary values  $\rho_{\text{min}} = 0.75\Omega\text{m}$  and  $\rho_{\text{max}} = 1.2\Omega\text{m}$  at water contents of 3 and 5%, respectively. b) Inferred rhyolite melt fraction based on a two-phase Archie's law (Glover et al. 2000) for  $\rho_{\text{min}}$  and  $\rho_{\text{max}}$  and melt interconnectivities representing the upper Hashin-Shtrikman-bound ( $m=1.15$ ) and crystalline mush ( $m=1.5$ ).**

The lower conductor, C4, likely represents a basaltic mush column that acts as the feeding zone of the Aluto magmatic system. The extent of this structure to depth and to the west cannot be further constraint by this study, due to the limited aperture of the survey layout. In an earlier study, Hübert et al. (2017) imaged a conductive zone on a 2-D transect across the rift west of Aluto with a similar dip angle. However, reliable constraints on the extent of C4 would require a 3-D study with a regular spatial site coverage across the rift. C4 follows the dip angle ( $65^\circ$ ) of large border faults and corresponds to the derived dip of slip planes from recorded earthquakes, which occur predominantly at depths  $<14\text{km}$  in this area of the MER (Keir et al., 2006; Corti, 2009). The geometry of C4 thus provides strong evidence for the existence of faults that extend throughout the entire crust, forming weak zones that channel melt ascent. The generally higher resistivities towards the eastern part of the rift (R2) suggest that the deep-reaching fault acts as a horizontal barrier between the more heterogeneous crust beneath the western plateau and the more intact and thicker crust beneath the eastern plateau, as observed in earlier studies (e.g. Whaler et al., 2006).

Fig. 5 shows a detailed EW slice of the upper 5km transecting Aluto at the productive wells LA3, LA6, LA9 and LA10. Conductor C1 shows an offset with a step upward across the AJFZ, which is indicated by the dashed line. This is in agreement with the well stratigraphy that revealed substantial offsets in the thermally altered Bofa basalt unit between the wells (Gianelli and Teklemariam, 1993). Below the clay cap, C1, no clear indications for lateral heterogeneities across the AJFZ are visible. One reason could be the limited resolution of MT data below conductors, or the limited frequency range used for this study. Note, we only inverted data up to a shortest period of 0.0173s (i.e.  $\sim 57\text{Hz}$ ). In a future study, we will include existing high frequency data up to 4000Hz to increase the resolution at shallow depths. The conductor C1 follows the outflow zone, as inferred from Wells LA7 and LA5. Wells LA3, LA6, LA9 and LA10 were drilled into the upflow zone and are characterized by a steady increase in temperature, with maximum temperatures exceeding 300°C (Gianelli and Teklemariam, 1993; Sisay, 2016).

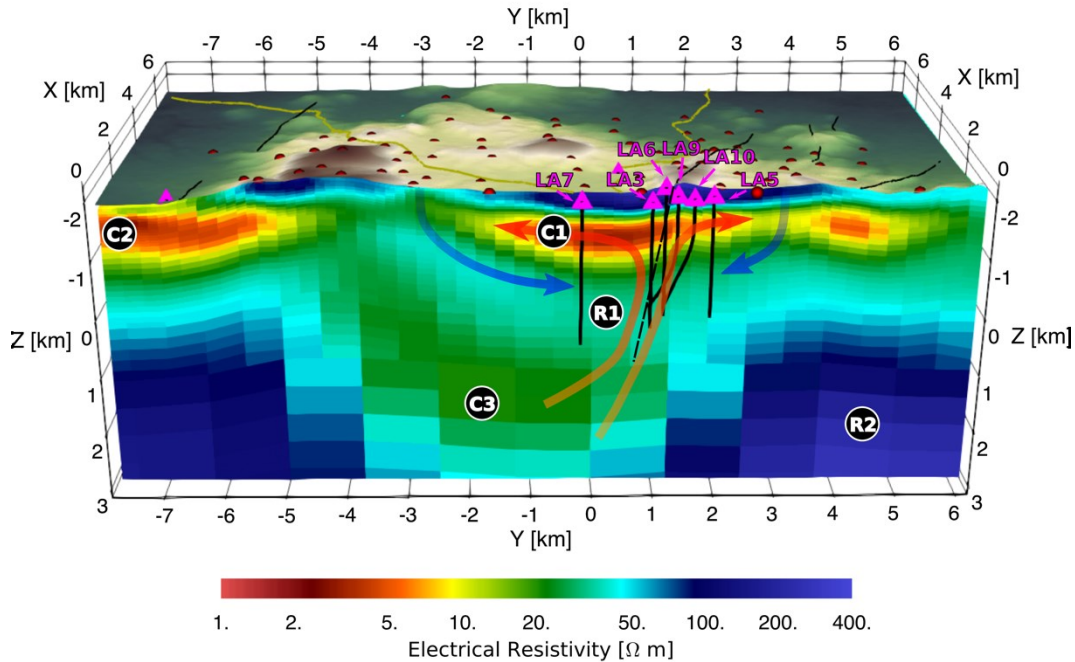


**Figure 5: Detailed EW-slice through the central part of Aluto, where the productive wells, LA3, LA6, LA9 and LA10, are located. The productive wells are drilled into the upflow zone, where hot fluids, that presumably originate from the crystalline mush zone, C3, migrate upwards along the permeable fault structure of the AJFZ (dashed line). At shallower depths, the geothermal fluids are deflected to the sides (red arrows), resulting in the formation of the hydrothermally altered clay cap. LA5 and LA7 are affected by a temperature reversal, due to inflow of cold meteoric water, as illustrated by the blue arrows.**

LA5 and LA7 were drilled into the outflow zone, both reach a maximum temperature of more than 200°C, at about 1000m -1500m depth. Towards greater depths, LA5 and LA7 are affected by a temperature reversal and inflow of cold meteoric water (Gianelli and Teklemariam, 1993). The zone with inflow of cold fluids, corresponds to a sub-horizontal feature of moderate electrical resistivities ( $\sim 50\ \Omega\text{m}$ ) that begins at the eastern and western sides of the clay cap. Beneath the western part of the clay cap this resistor extends until LA7, at a depth, where the well is affected by inflow of cold meteoric fluids. The related aquifer is situated within a permeable layer of Bofa basalts and tertiary ignimbrites. Fumarolic activity along the proposed caldera rim, west of LA7 and east of LA5, indicates a potential extent of this permeable zone, that might be the main hydrological unit responsible for groundwater recharge by meteoric waters. Strong rainfall during the Ethiopian rain season leads to the episodic formation of a caldera lake, as shown in Fig. 6. The lake covers the largest area of the Aluto caldera and might play an important role delivering meteoric water for recharging Aluto's hydrothermal system.

Our model supports recent hypotheses of deformation mechanisms at Aluto, that argue in favor of dynamic changes within the hydrothermal system, rather than deformation caused by magma emplacement itself (Samrock et al. 2016; Hutchison et al. 2016). The 3-D electrical conductivity model provides no evidence for the existence of a dynamic magmatic system with large amounts of melt and ongoing melt emplacement. Aluto's magmatic system shows similarities with the transcrustal magmatic-hydrothermal system as it was imaged under Tulu Moye 50km north of Aluto (Samrock et al., 2018). However, beneath Aluto, the magmatic system appears to be at a more mature and in a highly crystalline stage. The observed uplift events are most likely caused by episodic releases of hot, water-rich volatile fluids that are derived from the upper crustal crystalline mush zone (C3) or from greater depths (C4). Evidence for rapid heating events are provided by a study of Valori et al. (1992), who found that in-hole temperatures in LA3 and LA6 are almost 100°C higher than inferred from fluid inclusions, trapped in hydrothermally altered rocks in the same wells. These results confirm a conceptual model of Hutchison et al. (2016), who suggested that the magmatic and hydrothermal reservoirs of Aluto are connected and that magmatic volatiles are transported to the surface through faults and fracture pathways, leading to episodic volcanic unrest.

#### 4. CONCLUSION

The first 3-D inversion of the comprehensive MT data-set from Aluto, that was measured during three independent surveys, demonstrated that a spatially inclusive and comprehensive data coverage as well as state-of-the-art numerical tools are crucial in order to sense and image the entire trans-crustal magmatic and hydrothermal system under Aluto. New insights about the magmatic

plumbing system beneath Aluto provide answers to the previously enigmatic nature of the mechanisms that drive volcanic unrest under Ethiopia's only power-producing geothermal field.



**Figure 6: View towards the west over the Aluto caldera in the direction of Wells LA3 and LA7. The photo shows a caldera lake, which formed after rainfalls in May 2016. The lake has a diameter of approx. 1.3km. The photo was taken by the author.**

#### REFERENCES

- Birhanu, Y., Bendick, R., Fisseha, S., Lewi, E., Floyd, M., King, R., & Reilinger, R. (2016). GPS constraints on broad scale extension in the Ethiopian Highlands and Main Ethiopian Rift. *Geophysical Research Letters*, 43, 6844–6851.
- Biggs, J., Bastow, I. D., Keir, D., & Lewi, E. (2011). Pulses of deformation reveal frequently recurring shallow magmatic activity beneath the Main Ethiopian Rift. *Geochemistry, Geophysics, Geosystems*, 12, Q0AB10.
- Caldwell, T. G., Bibby, H. M., & Brown, C. (2004). The magnetotelluric phase tensor. *Geophysical Journal International*, 158(2), 457–469.
- Casu, F., Elefante, S., Imperatore, P., Zinno, I., Manunta, M., De Luca, C., & Lanari, R. (2014). SBAS-DInSAR parallel processing for deformation time-series computation. *IEEE Journal of Selected Topics in Applied Earth Observations and Remote Sensing*, 7(8), 3285–3296.
- Cherkose, Biruk Abera, and Hideki Mizunaga. Resistivity imaging of Aluto-Langano geothermal field using 3-D magnetotelluric inversion. *Journal of African Earth Sciences* 139 (2018): 307-318.
- Cherkose, Biruk Abera, Hideki Mizunaga, and F. Samrock. Imaging Resistivity Structures of High-Enthalpy Geothermal Systems Using Magnetotelluric Method: A case study of Aluto-Langano geothermal field in Ethiopia. *Proceedings, 7th African Rift Geothermal Conference*, Kigali, Rwanda 31st October – 2nd November 2018.
- Corti, G. (2009). Continental rift evolution: From rift initiation to incipient break-up in the Main Ethiopian Rift, East Africa. *Earth-Science Reviews*, 96(1), 1–53.
- Gianelli, G. & Teklemariam, M., 1993. Water-rock interaction processes in the Aluto-Langano geothermal field (Ethiopia), *Journal of Volcanology and Geothermal Research*, 56(4), 429–445.
- Gleeson, M. L., Stock, M. J., Pyle, D. M., Mather, T. A., Hutchison, W., Yirgu, G., & Wade, J. (2017). Constraining magma storage conditions at a restless volcano in the Main Ethiopian Rift using phase equilibria models. *Journal of Volcanology and Geothermal Research*, 337, 44–61.
- Glover, P. W., Hole, M. J., & Pous, J. (2000). A modified Archie's law for two conducting phases. *Earth and Planetary Science Letters*, 180(3-4), 369–383.
- Grayver, A. V. (2015). Parallel three-dimensional magnetotelluric inversion using adaptive finite-element method. Part I: Theory and synthetic study. *Geophysical Journal International*, 202(1), 584–603.
- Grayver, A. V., van Driel, M., & Kuvshinov, A. V. (2019). Three-dimensional magnetotelluric modelling in spherical Earth. *Geophysical Journal International*, 217(1), 532-557.
- Guo, X., Zhang, L., Behrens, H., & Ni, H. (2016). Probing the status of felsic magma reservoirs: Constraints from the P–T–H<sub>2</sub>O dependences of electrical conductivity of rhyolitic melt. *Earth and Planetary Science Letters*, 433, 54–62.

- Hochstein, M. P., Oluma, B., & Hole, H. (2017). Early exploration of the Aluto geothermal field, Ethiopia (History of discovery well LA-3). *Geothermics*, 66, 73-84.
- Hübner, J., Whaler, K., & Fisseha, S. (2018). The electrical structure of the central main Ethiopian Rift as imaged by magnetotellurics: implications for magma storage and pathways. *Journal of Geophysical Research: Solid Earth*, 123(7), 6019-6032.
- Hutchison, W., Mather, T. A., Pyle, D. M., Biggs, J., & Yirgu, G. (2015). Structural controls on fluid pathways in an active rift system: A case study of the Aluto volcanic complex. *Geosphere*, 11(3), 542-562.
- Hutchison, W., Biggs, J., Mather, T. A., Pyle, D. M., Lewi, E., Yirgu, G., et al. (2016). Causes of unrest at silicic calderas in the East African Rift: New constraints from InSAR and soil-gas chemistry at Aluto volcano, Ethiopia. *Geochemistry, Geophysics, Geosystems*, 17, 3008–3030.
- Jiracek, G. R. (1990). Near-surface and topographic distortions in electromagnetic induction. *Surveys in Geophysics*, 11(2-3), 163-203.
- Johnston, J., Pellerin, L. & Hohmann, G., 1992. Evaluation of electromagnetic methods for geothermal reservoir detection, *Transactions-Geothermal Resources Council*, 16, 241–245.
- Käuffl, J. S., Grayver, A. V., & Kuvshinov, A. V. (2018). Topographic distortions of magnetotelluric transfer functions: A high-resolution 3-D modelling study using real elevation data. *Geophysical Journal International*, 215(3), 1943–1961.
- Kebede, S. (2016). Country update on geothermal exploration and development in Ethiopia. *Proceedings, 6th African Rift Geothermal Conference (pp. 1–15)*. Addis Ababa, Ethiopia.
- Keir, D., Ebinger, C. J., Stuart, G. W., Daly, E., & Ayele, A. (2006). Strain accommodation by magmatism and faulting as rifting proceeds to breakup: Seismicity of the northern Ethiopian rift. *Journal of Geophysical Research*, 111, B05314.
- Lévy, L., Gibert, B., Sigmundsson, F., Flóvenz, Ó. G., Hersir, G. P., Briole, P., & Pezard, P. (2018). The role of smectites in the electrical conductivity of active hydrothermal systems: Electrical properties of core samples from Krafla volcano, Iceland. *Geophysical Journal International*, 215, 1558–1582.
- Rizzello, D., Armadillo, E., Verdoya, M., Pasqua, C., Kebede, S., Mengiste, A., ... & Meqbel, N. (2017, April). Integrated geophysical imaging of the Aluto-Langano geothermal field (Ethiopia). *EGU General Assembly Conference Abstracts* (Vol. 19, p. 17959).
- Sisay, S. W. (2016). Sub-surface geology and hydrothermal alteration of wells LA9D and LA10D of Aluto-Langano geothermal field, Ethiopia. *Proceedings, 6th African Rift Geothermal Conference, Addis Ababa, Ethiopia, 2nd–4th November 2016*
- Samrock, F., Kuvshinov, A., Bakker, J., Jackson, A., & Fisseha, S. (2015). 3-D analysis and interpretation of magnetotelluric data from the Aluto-Langano geothermal field, Ethiopia. *Geophysical Journal International*, 202(3), 1923–1948.
- Samrock, F., Grayver, A. V., Eysteinnsson, H., & Saar, M. O. (2018). Magnetotelluric image of transcrustal magmatic system beneath the Tulu Moye geothermal prospect in the Ethiopian Rift. *Geophysical Research Letters*, 45(23), 12-847.
- Simpson, F., & Bahr, K. (2005). *Practical magnetotellurics*. Cambridge: Cambridge University Press.
- Tietze, K., Ritter, O., & Egbert, G. D. (2015). 3-D joint inversion of the magnetotelluric phase tensor and vertical magnetic transfer functions. *Geophysical Journal International*, 203(2), 1128-1148.
- Valori, A., Teklemariam, M., & Gianelli, G. (1992). Evidence of temperature increase of CO<sub>2</sub>-bearing fluids from Aluto-Langano geothermal field (Ethiopia): a fluid inclusions study of deep wells LA-3 and LA-6. *European Journal of Mineralogy*, 907-920.